

Quantum liquid crystals in the finite-field $K\Gamma$ model for α - RuCl_3

Masahiko G. Yamada^{1,*} and Satoshi Fujimoto^{1,2}

¹*Department of Materials Engineering Science, Osaka University, Toyonaka 560-8531, Japan*

²*Center for Quantum Information and Quantum Biology, Osaka University, Toyonaka 560-8531, Japan*

(Dated: November 22, 2021)

We study the extended Kitaev model called the $K\Gamma$ model, using a perturbative expansion combined with a well-controlled mean-field approximation and a cutting-edge exact diagonalization. In the phase diagram, we discover a nematic Kitaev spin liquid and a Kekulé Kitaev spin liquid. The former potentially explains the high-field nematic state with zero Chern number experimentally observed in α - RuCl_3 , even for sufficiently small values of $\Gamma/|K|$. The latter has a Majorana zero mode in its Z_3 vortex core, which can be potentially controlled by the domain wall motion. This opens a possible application of the quantum liquid crystal phases in the $K\Gamma$ model to the topological quantum computation.

Introduction. — The Kitaev model [1] is a prominent example of exactly solvable models with a quantum spin liquid (QSL) property, which is characterized by various topological signatures [2, 3]. However, it is known that real materials cannot fully be described by this fine-tuned model and include additional interactions [4], which potentially change the topological property of the ground state. Recently the $K\Gamma$ model [5–17] has been investigated intensively in connection with a Kitaev material α - RuCl_3 , and various kinds of topological transitions were expected theoretically. Whereas various numerical methods have been used, most studies treat itinerant Majorana fermions of the Kitaev model indirectly, and the role of Majorana fermions is unclear.

Among many possible realizations of the proximate Kitaev model [18–24], α - RuCl_3 is an outstanding material because a half-integer quantization of the thermal Hall conductivity has been observed [25, 26]. At higher field, the breaking of the threefold rotation symmetry has been observed from the field angle dependence of the heat capacity at the same time as the disappearance of the thermal Hall effect [27]. The coincidence is attributed to the first-order transition from Kitaev’s B phase with a Chern number 1 to Kitaev’s A phase with a Chern number 0, which occurs directly maintaining an energy gap [28]. A theoretical characterization is necessary for the high-field nematic phase based on a microscopic model like the $K\Gamma$ model. While some studies [6, 12] find the nematic phase within the $K\Gamma$ model, the property of the associated nematic phase transition from the Kitaev spin liquid is not well discussed [14].

Another interesting phase with a broken threefold rotation symmetry is a Kekulé phase. Though both a nematic phase and a Kekulé phase are Z_2 spin liquids with a toric code topological order, some properties are different. The most significant difference is the presence of a Majorana zero mode (MZM) in the Z_3 vortex for a Kekulé phase [29, 30]. Here a Z_3 vortex means a crossing point of boundaries of three different domains of the Z_3 -broken Kekulé phases. MZMs can potentially be braided by the domain wall motion, which leads to a nontriv-

ial phase. Thus, by controlling such topological defects in this liquid crystalline phase, the protected quantum computation in the MZM states is possible.

Both of these phases are relevant to the $K\Gamma$ model even in the mean-field level, and thus we investigate these phases precisely. From now on we call the nematic phase nematic Kitaev spin liquid (NKSL) and the Kekulé phase Kekulé-Kitaev spin liquid (KKSL).

From the mean-field approximation and the exact diagonalization, we discover a vast region of NKSL and KKSL with a broken threefold rotation symmetry. Both of these phases can be regarded as quantum spin analogues of liquid crystals [31]. These phases are enabled to be discovered by the methods which treat itinerant Majorana fermions directly.

In this Letter, we study a phase diagram of the finite-field $K\Gamma$ model using the third-order perturbation. The effective model is an interacting Majorana model with four-body and six-body interactions [32–41]. Based on the mean-field solution and the exact diagonalization, we find the phase diagram is rich enough to predict various exotic spin liquids like NKSL and KKSL.

Third-order perturbation. — We begin with the following Kitaev- Γ or $K\Gamma$ model. These two terms are known to be dominant in α - RuCl_3 .

$$\begin{aligned} H_0 &= K \sum_{\langle ij \rangle \in \alpha\beta(\gamma)} S_i^\gamma S_j^\gamma + \Gamma \sum_{\langle ij \rangle \in \alpha\beta(\gamma)} (S_i^\alpha S_j^\beta + S_i^\beta S_j^\alpha) \\ &= -\frac{|K|}{4} \sum_{\langle ij \rangle \in \alpha\beta(\gamma)} \sigma_i^\gamma \sigma_j^\gamma + \frac{\Gamma}{4} \sum_{\langle ij \rangle \in \alpha\beta(\gamma)} (\sigma_i^\alpha \sigma_j^\beta + \sigma_i^\beta \sigma_j^\alpha), \end{aligned} \quad (1)$$

where we assume $K < 0$, and Γ to be a real number, and S_i and σ_i are spin-1/2 and Pauli operators defined on the i th site, respectively. $\langle ij \rangle \in \alpha\beta(\gamma)$ means that a nearest-neighbor (NN) bond $\langle ij \rangle$ belongs to γ -bonds as shown in Fig. 1(a), and the $\alpha\beta$ -plane is perpendicular to the γ -direction. We note that our study is based on the original Kitaev model with an additional interaction, not the so-called Kekulé-Kitaev model [42–44]. The Kekulé-Kitaev model explicitly breaks the Z_3 symmetry, while

our model spontaneously breaks this symmetry in the Kekulé phase.

As is usually the case, the nontrivial contribution begins from the third order in Γ/K . The third-order perturbation leads to the following effective Hamiltonian.

$$H_{\text{eff}} = \frac{6\Gamma^3}{0.21|K|^2} \sum_{\langle ij \rangle \langle kl \rangle \langle mn \rangle \in \diamond} (\sigma_i^x \sigma_j^y + \sigma_i^y \sigma_j^x) \times (\sigma_k^y \sigma_l^z + \sigma_k^z \sigma_l^y) (\sigma_m^z \sigma_n^x + \sigma_m^x \sigma_n^z), \quad (2)$$

where $\langle ij \rangle \langle kl \rangle \langle mn \rangle \in \diamond$ means that $\langle ij \rangle$, $\langle kl \rangle$, and $\langle mn \rangle$ are two possible patterns for z -, x -, and y -bonds, respectively, inside each hexagon. The factor $0.21 \sim 4 \times 0.227^2$ comes from the intermediate vortex pattern [28, 45], as shown in Fig. 1(b).

We then move on to the effective Majorana interacting model.

$$H_c = \frac{t}{4} \sum_{\langle ij \rangle} i c_i c_j - \frac{6\Gamma^3}{0.21|K|^2} \sum_{\langle ijkl \rangle} c_i c_j c_k c_l - \frac{12\Gamma^3}{0.21|K|^2} \sum_{\langle ijklmn \rangle} i c_i c_j c_k c_l c_m c_n, \quad (3)$$

where $t \propto |K| + O(\Gamma^2/|K|)$, $\langle ijkl \rangle$ represents armchair-type interactions shown in Fig. 1(c), and $\langle ijklmn \rangle$ represents six-body interactions shown in Fig. 1(d). The site ordering of $\langle ijkl \rangle$ and $\langle ijklmn \rangle$ is counterclockwise, as shown in Figs. 1(c)-(d).

The same process applies to the case with a magnetic field. We can consider the Hamiltonian $H = H_0 + H_1$ with

$$H_1 = - \sum_j (h^x S_j^x + h^y S_j^y + h^z S_j^z) = - \sum_j \left(\frac{h^x}{2} \sigma_j^x + \frac{h^y}{2} \sigma_j^y + \frac{h^z}{2} \sigma_j^z \right), \quad (4)$$

where $\vec{h} = (h^x, h^y, h^z)^t$ is an applied magnetic field. By tracking intermediate vortex states, we would finally get

$$H'_c = \frac{t}{4} \sum_{\langle ij \rangle} i c_i c_j - \frac{12\Gamma^3}{0.21|K|^2} \sum_{\langle ijklmn \rangle} i c_i c_j c_k c_l c_m c_n - \sum_{\langle ijkl \rangle \in \alpha\beta(\gamma)} \left(\frac{6h^\alpha h^\beta \Gamma}{0.060|K|^2} + \frac{6\Gamma^3}{0.21|K|^2} \right) c_i c_j c_k c_l + \sum_{\langle\langle ij \rangle\rangle \in \alpha\beta(\gamma)} \frac{12h^\alpha h^\beta \Gamma}{0.060|K|^2} i c_i c_j + \frac{6h^x h^y h^z}{0.035|K|^2} \sum_{\langle\langle ij \rangle\rangle} i c_i c_j + \frac{6h^x h^y h^z}{0.035|K|^2} \left(\sum_{\langle\langle ijkl \rangle\rangle_\lambda} c_i c_j c_k c_l - \sum_{\langle\langle ijkl \rangle\rangle_\gamma} c_i c_j c_k c_l \right), \quad (5)$$

where $t \propto |K| + O(\Gamma^2/|K|) + O(h^2/|K|)$, $\langle ijkl \rangle \in \alpha\beta(\gamma)$ means that a bond $\langle jk \rangle$ belongs to γ -bonds with the $\alpha\beta$ -plane perpendicular to the γ -direction, $\langle\langle ij \rangle\rangle$ represents

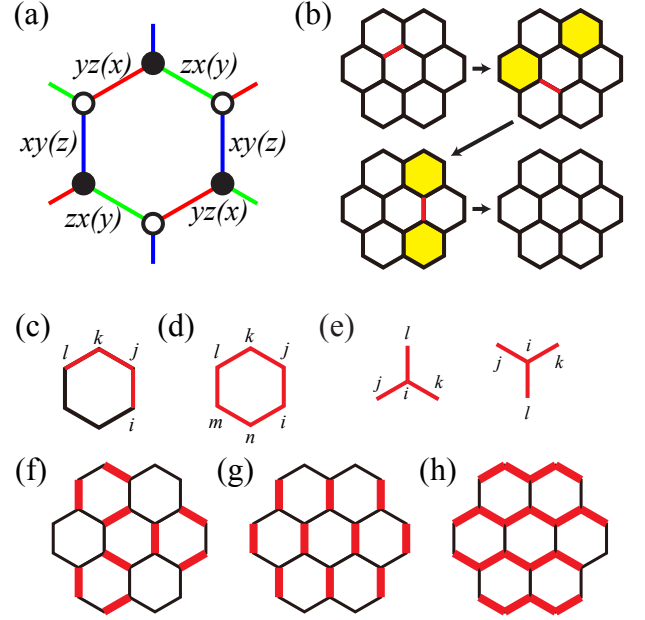


FIG. 1. (a) Honeycomb lattice where the KT model is defined. Red, green, and blue bonds represent bonds in the x -, y -, and z -directions, respectively. (b) Example of intermediate states with an energy $0.227|K|/4$ in the third-order perturbation. (c) Example of armchair-type four-body interactions shown in red bonds. All six symmetry-equivalent terms are included in the Hamiltonian. (d) Six-body plaquette interaction shown in red. (e) λ -shaped and γ -shaped four-body interactions shown in red. (f) Kekulé bond order with strong bonds shown in red. (g) Nematic bond order with strong bonds shown in red. (h) Zigzag nematic bond order with strong bonds shown in red.

a next-nearest-neighbor (NNN) bond, and $\langle\langle ijkl \rangle\rangle$ represents a λ -shaped, or γ -shaped interaction for sites $ijkl$, where ij , jk , and il are connected by x -, y -, and z -bonds, respectively, as shown in Fig 1(e). $\langle\langle ij \rangle\rangle \in \alpha\beta(\gamma)$ means the next-next-nearest-neighbor (NNNN) bond which is a diagonal of hexagons in the γ -direction, where i is even and j is odd as usual.

From now on, we set $h^x = h^y = h^z = h/\sqrt{3}$ for simplicity. The absolute value of t is undecidable, so we set $t = 1$ as a simple normalization. We note that two-body terms are not antisymmetrized, so the hopping amplitude is $1/8$ in the Hermitian form.

The tqs model. — Let us begin with the zero-field model. First, we extend the model to the following form:

$$H_{tqs} = \frac{t}{4} \sum_{\langle ij \rangle} i c_i c_j - q \sum_{\langle ijkl \rangle} c_i c_j c_k c_l - 2s \sum_{\langle ijklmn \rangle} i c_i c_j c_k c_l c_m c_n, \quad (6)$$

with q and s being real parameters. When $q = s = 6\Gamma^3/(0.21|K|^2)$, this tqs model becomes the original (KT) model with $h = 0$.

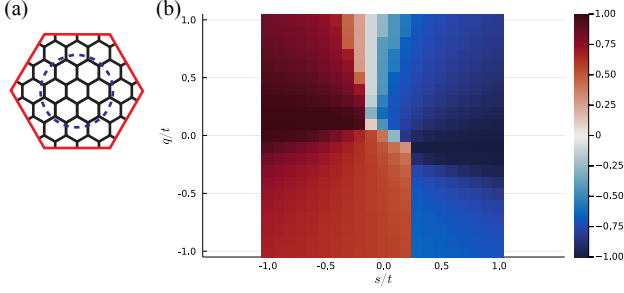


FIG. 2. (a) 54-site cluster with a periodic boundary condition used in the exact diagonalization. A blue dashed circle shows an entanglement cut for the calculation of the entanglement entropy. (b) Expectation value of V_p of the tqs model computed by exact diagonalization.

The operator

$$V_p = -ic_i c_j c_k c_l c_m c_n. \quad (7)$$

can be defined for each hexagon plaquette $p = \langle ijklmn \rangle$, and plays an important role as they commute with each other. Indeed, the tqs model is integrable in the limit $|s| \rightarrow \infty$. Eigenstates are constructed by assigning $V_p = \pm 1$ for each plaquette.

This limit ($|s| \rightarrow \infty$) is also known as the Vijay-Hsieh-Fu (VHF) surface code [33] and has a characteristic Z_2 topological order with an exact S_3 anyon symmetry. To check the existence of such a phase we did exact diagonalization of the 54-site cluster, which is shown in Fig. 2(a). This VHF surface code is indeed realized in the tqs model with a large $|s|$ region, as shown in Fig. 2(b). In Fig. 2(b) the right half is mostly blue connected to the $s \rightarrow \infty$ limit, and the left half is mostly red connected to the $s \rightarrow \infty$ limit. This means that the large $|s|$ phase is rather stable with respect to the perturbation of t and q .

It seems that even on the $q = s$ line, most of the $q > 0$ region is connected to this VHF surface code phase, and from this we conclude that even in the original (KT) model Eq. (5) this phase is realized in the large $\Gamma/|K|$ region. Since the resolution of Fig. 2(b) is not good enough, the exact region of $\Gamma/|K|$ where this phase is realized will be discussed later.

KT model with a magnetic field. — Then, we go back to the original (KT) model Eq. (5). With a magnetic field, it indeed becomes easy to identify the phase because we can use a Chern number to diagnose gapped topological phases. The Chern number is connected to the topological order of the spin model according to Kitaev's 16-fold way. For example, phases with a Chern number ± 1 in the Majorana model can be identified with the Ising topological order, which we call a chiral spin liquid (CSL) with a Chern number ± 1 in the following.

The mean-field phase diagram is shown in Fig. 3(a) Phases are identified from the Chern number and bond

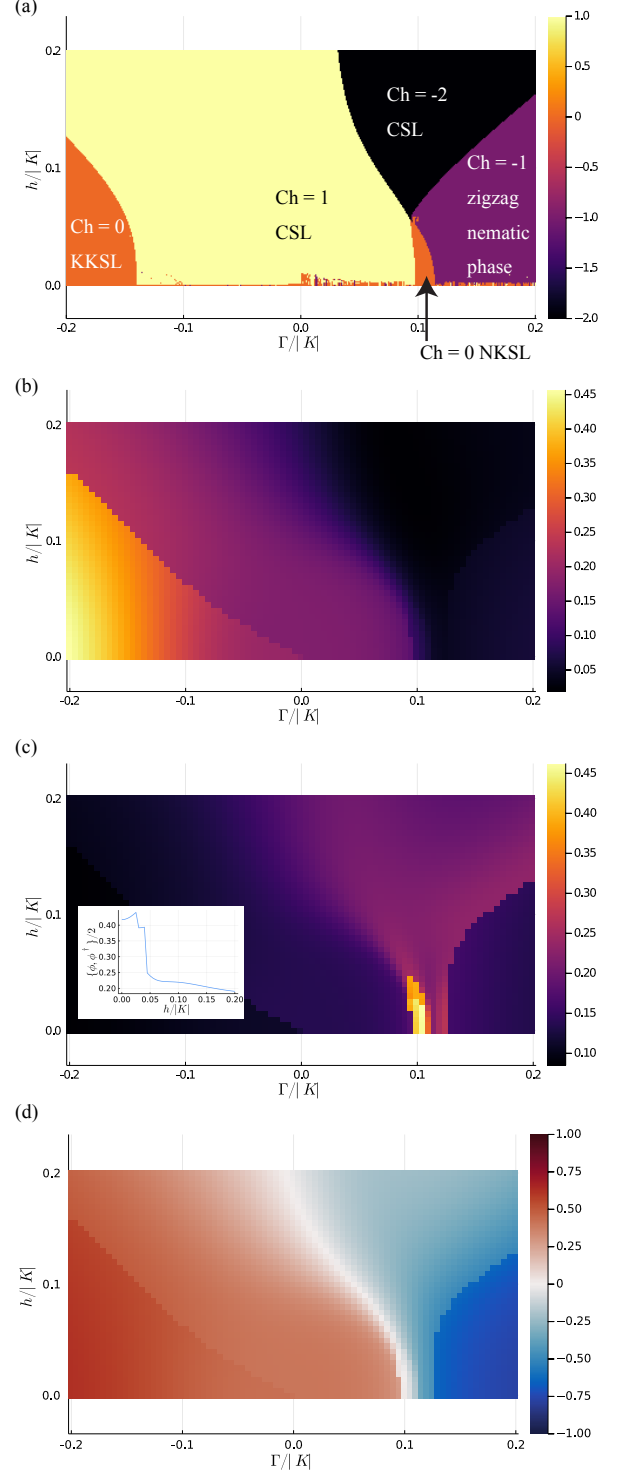


FIG. 3. (a) Mean-field phase diagram of the KT model. The color plot shows the value of the Chern number (Ch). (b) Hermitian version of a Kekulé order parameter $\{\psi, \psi^\dagger\}/2$ computed by exact diagonalization. (c) Hermitian version of a nematic order parameter $\{\phi, \phi^\dagger\}/2$ computed by exact diagonalization. The inset shows $\{\phi, \phi^\dagger\}/2$ on the line $h/|K| = 0.1$. The value clearly drops from around 0.4 to 0.25 at the transition point. (d) V_p computed by exact diagonalization.

order parameters. The Chern number is computed by the Fukui-Hatsugai-Suzuki method [46]. The details of the calculation is included in Supplemental Material (SM) [47]. The method is based on Refs. [28, 35]. From the phase diagram we find the following phases:

1. a KKSL with a Chern number 0.
2. Kitaev's non-Abelian CSL with a Chern number 1.
3. an Abelian CSL with a Chern number -2 .
4. an NKSL with a Chern number 0.
5. a zigzag nematic phase with a Chern number -1 .

The bond ordering patterns for a KKSL, an NKSL, and a zigzag nematic phase are shown in Figs. 1(f), (g), and (h), respectively.

Exact diagonalization. — From now on we will confirm the results of the mean-field theory by exact diagonalization of Eq. (5). The exact diagonalization is done using the 54-site cluster again. We note that this size is much larger than what has been used for the Kitaev model exact diagonalization. We take an average of expectation values for all the degenerate ground states. First, we check the operator $\{\psi, \psi^\dagger\}/2$, corresponding to the absolute value of the Kekulé order parameter [48] with

$$\psi = \Delta'_1 + e^{2\pi i/3} \Delta'_2 + e^{4\pi i/3} \Delta'_3, \quad (8)$$

where the definition of Δ'_i ($i = 1-9$) is included in SM [47]. In Fig. 3(b), the orange triangular region with $\Gamma < 0$ corresponds to the Kekulé-ordered phase. The area of this phase becomes larger than that of the mean-field phase diagram. Surprisingly, it looks like the Kekulé order appears with an infinitesimal $\Gamma < 0$ in the 54-site calculation. This implies that the Kitaev spin liquid is unstable with respect to a negative Γ perturbatively and it is possible that the Kekulé order opens a gap for Dirac cones (see SM [47] for more details).

Next we check the nematic order parameter $\{\phi, \phi^\dagger\}/2$ [48] with

$$\psi = \Delta_1 + e^{2\pi i/3} \Delta_2 + e^{4\pi i/3} \Delta_3, \quad (9)$$

where the definition of Δ_i ($i = 1-9$) is included in SM [47]. In Fig. 3(c), NKSL is identified with the small orange region around $\Gamma/|K| = 0.1$. The area of this phase becomes smaller than that of the mean-field phase diagram. We now confirmed the existence of NKSL even in the exact diagonalization, but the zigzag nematic phase disappears in the same calculations. There remains a violet region which is different from the zigzag nematic phase found in the mean-field approach. We note that the order parameter is nonzero on the whole parameter space in Fig. 3(b) and (c) due to the finite-size effect.

Finally, we check the value of V_p to identify the mysterious area which cannot be identified by the calculation

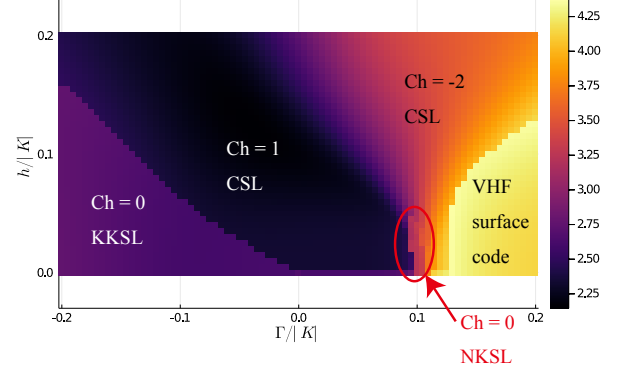


FIG. 4. Phase diagram obtained from the 54-site exact diagonalization of the KT model. The color plot shows the value of the entanglement entropy. The entanglement cut is shown in Fig. 2(a) by the blue dashed circle (see also SM [47]).

of the nematic order parameter. As shown in Fig. 3(d), the value of $|V_p|$ reaches around 0.75, which is very close to the highest value $+1$. Combined with what is obtained from the tqs model, we believe that this phase is connected to the large $|s|$ phase of the tqs model. Thus, this phase appearing in the large $\Gamma/|K|$ region should be described by the VHF surface code. This region indeed has the largest value of the entanglement entropy (see Fig. 4), which reconfirms that it is a highly entangled phase which cannot be described by the mean-field picture.

Phase diagram of the KT model. — As shown in Fig. 4, we find the following phases.

1. a KKSL with a Chern number 0.
2. Kitaev's non-Abelian CSL with a Chern number 1.
3. an Abelian CSL with a Chern number -2 .
4. an NKSL with a Chern number 0.
5. a VHF surface code.

Except for the fact that the zigzag nematic phase is replaced by the VHF surface code, the phases obtained are the same as those found in the mean-field theory. We note that Kitaev's non-Abelian CSL with a Chern number 1 is identified because this phase is stable on the $\Gamma/|K| = 0$ line [28], while an Abelian CSL with a Chern number -2 is just a speculation.

Especially in the experimentally relevant region, $\Gamma/|K| \sim 0.1$, we find an NKSL phase with a Chern number 0, which potentially explains the observed topological nematic transition from Kitaev's non-Abelian CSL to the toric code phase.

Overall, we have obtained a very rich phase diagram within the flux-free assumption, and disclosed the existence and properties of NKSL expected from experiments. Though our calculation is somewhat idealized, a

more realistic phase diagram should be obtained by dealing with a Γ' term, for example, additionally [49, 50]. In addition, in the future it is important to check whether an Abelian CSL with a Chern number -2 is connected to the one discovered previously in the $K\Gamma'$ model [50].

Effect of the Heisenberg term. — Here we will discuss the effect of the Heisenberg term. With this term the third-order perturbation leads to the following additional interaction.

$$H'_{\text{eff}} \propto \frac{\hbar^2 J}{|K + J|^2} \left(\sum_{\langle\langle\langle ijkl \rangle\rangle\rangle} c_i c_j c_k c_l \pm \sum_{\langle\langle\langle ij \rangle\rangle\rangle'} i c_i c_j \right), \quad (10)$$

where $\langle\langle\langle ijkl \rangle\rangle\rangle$ represents an zigzag-type interaction for sites $ijkl$, and $\langle\langle\langle ij \rangle\rangle\rangle'$ represents an NNNN hopping which is not a diagonal of hexagons. This term promotes nematic order, and potentially enhances NKSL. Thus, the additional small Heisenberg term should be relevant to the field-induced nematic transition, and will be investigated in the future.

Discussion. — We invent a systematic approach to treat non-Kitaev interactions in a perturbative manner by fully incorporating many-body effects of Majorana interactions. We discover the emergence of a Kekulé order in the $K\Gamma$ model for $\Gamma < 0$, and a nematic order for $\Gamma > 0$, as well as a more exotic VHF surface code phase. We also discover an Abelian CSL with a Chern number -2 , which can be detected by the sign change of the thermal Hall effect or spin Seebeck effect [51].

In the experimentally relevant region $\Gamma/|K| \sim 0.1$ for $\alpha\text{-RuCl}_3$, the discovered nematic phase potentially explains the nematic transition observed in the high-field phase. While the position of the NKSL phase $\Gamma/|K| \sim 0.1$ is consistent the density matrix renormalization group [6, 14], its nature is totally different from nematic phases discovered previously [12]. NKSL is not a simple nematic phase but a spin liquid phase with a partial symmetry breaking. We believe that NKSL discovered in our study is not the same phase as the ones in the previous studies, and that the approximate coincidence of the nematic region $\Gamma/|K| \sim 0.1$ is only accidental. Our study endorses the topological nematic transition scenario proposed in Ref. [28] with a more realistic model and interactions. This state is potentially detectable by nuclear magnetic resonance (NMR) or Mössbauer spectroscopy [52].

Another direction to explore is to engineer the Kekulé order in artificial systems. The sign and magnitude of the Γ term is known to be strongly dependent on the spin-orbit coupling (SOC), so it can potentially be controlled by the proximity effect with a substrate. The substrate with heavy elements may strengthen the SOC of $\alpha\text{-RuCl}_3$, and allow the fine tuning of Γ . The signature of the Kekulé phase is the existence of an MZM at the Z_3 vortex core, which would potentially be discovered by scanning tunneling microscope (STM), leading

to a possible topological quantum computation.

We thank M. Gohlke, I. Kimchi, Y. Tada, M. O. Takahashi, D. Takikawa for fruitful discussions. This work was supported by JSPS KAKENHI Grant No. JP21H01039, and by JST CREST Grant Number JP-MJCR19T5, Japan. M.G.Y. is supported by Multidisciplinary Research Laboratory System for Future Developments, Osaka University. This research was supported in part by the National Science Foundation under Grant No. NSF PHY-1748958. The computation in this work has been done using the facilities of the Supercomputer Center, the Institute for Solid State Physics, the University of Tokyo.

* myamada@mp.es.osaka-u.ac.jp

- [1] A. Kitaev, Ann. Phys. **321**, 2 (2006), january Special Issue.
- [2] K. O'Brien, M. Hermanns, and S. Trebst, Phys. Rev. B **93**, 085101 (2016).
- [3] M. G. Yamada, Phys. Rev. Research **3**, L012001 (2021).
- [4] Y. Wang, G. B. Osterhoudt, Y. Tian, P. Lampen-Kelley, A. Banerjee, T. Goldstein, J. Yan, J. Knolle, H. Ji, R. J. Cava, J. Nasu, Y. Motome, S. E. Nagler, D. Mandrus, and K. S. Burch, npj Quantum Mater. **5**, 14 (2020).
- [5] J. G. Rau, E. K.-H. Lee, and H.-Y. Kee, Phys. Rev. Lett. **112**, 077204 (2014).
- [6] M. Gohlke, G. Wachtel, Y. Yamaji, F. Pollmann, and Y. B. Kim, Phys. Rev. B **97**, 075126 (2018).
- [7] A. Catuneanu, Y. Yamaji, G. Wachtel, Y. B. Kim, and H.-Y. Kee, npj Quantum Mater. **3**, 23 (2018).
- [8] Z.-X. Liu and B. Normand, Phys. Rev. Lett. **120**, 187201 (2018).
- [9] A. M. Samarakoon, G. Wachtel, Y. Yamaji, D. A. Tennant, C. D. Batista, and Y. B. Kim, Phys. Rev. B **98**, 045121 (2018).
- [10] J. S. Gordon, A. Catuneanu, E. S. Sørensen, and H.-Y. Kee, Nat. Commun. **10**, 2470 (2019).
- [11] L. E. Chern, R. Kaneko, H.-Y. Lee, and Y. B. Kim, Phys. Rev. Research **2**, 013014 (2020).
- [12] H.-Y. Lee, R. Kaneko, L. E. Chern, T. Okubo, Y. Yamaji, N. Kawashima, and Y. B. Kim, Nat. Commun. **11**, 1639 (2020).
- [13] T. Yamada, T. Suzuki, and S.-i. Suga, Phys. Rev. B **102**, 024415 (2020).
- [14] M. Gohlke, L. E. Chern, H.-Y. Kee, and Y. B. Kim, Phys. Rev. Research **2**, 043023 (2020).
- [15] F. L. Buessen and Y. B. Kim, Phys. Rev. B **103**, 184407 (2021).
- [16] Q. Luo, J. Zhao, H.-Y. Kee, and X. Wang, npj Quantum Mater. **6**, 57 (2021).
- [17] S.-S. Zhang, G. B. Halász, W. Zhu, and C. D. Batista, Phys. Rev. B **104**, 014411 (2021).
- [18] G. Jackeli and G. Khaliullin, Phys. Rev. Lett. **102**, 017205 (2009).
- [19] K. W. Plumb, J. P. Clancy, L. J. Sandilands, V. V. Shankar, Y. F. Hu, K. S. Burch, H.-Y. Kee, and Y.-J. Kim, Phys. Rev. B **90**, 041112 (2014).
- [20] M. G. Yamada, H. Fujita, and M. Oshikawa, Phys. Rev. Lett. **119**, 057202 (2017).

- [21] M. G. Yamada, V. Dwivedi, and M. Hermanns, Phys. Rev. B **96**, 155107 (2017).
- [22] H. Liu and G. Khaliullin, Phys. Rev. B **97**, 014407 (2018).
- [23] R. Sano, Y. Kato, and Y. Motome, Phys. Rev. B **97**, 014408 (2018).
- [24] S.-H. Jang, R. Sano, Y. Kato, and Y. Motome, Phys. Rev. B **99**, 241106 (2019).
- [25] Y. Kasahara, T. Ohnishi, Y. Mizukami, O. Tanaka, S. Ma, K. Sugii, N. Kurita, H. Tanaka, J. Nasu, Y. Motome, T. Shibauchi, and Y. Matsuda, Nature **559**, 227 (2018).
- [26] T. Yokoi, S. Ma, Y. Kasahara, S. Kasahara, T. Shibauchi, N. Kurita, H. Tanaka, J. Nasu, Y. Motome, C. Hickey, S. Trebst, and Y. Matsuda, Science **373**, 568 (2021).
- [27] O. Tanaka, Y. Mizukami, R. Harasawa, K. Hashimoto, N. Kurita, H. Tanaka, S. Fujimoto, Y. Matsuda, E.-G. Moon, and T. Shibauchi, (2020), arXiv:2007.06757 [cond-mat.str-el].
- [28] M. O. Takahashi, M. G. Yamada, D. Takikawa, T. Mizushima, and S. Fujimoto, Phys. Rev. Research **3**, 023189 (2021).
- [29] R. Jackiw and P. Rossi, Nucl. Phys. B **190**, 681 (1981).
- [30] Z.-C. Yang, T. Iadecola, C. Chamon, and C. Mudry, Phys. Rev. B **99**, 155138 (2019).
- [31] S. A. Kivelson, E. Fradkin, and V. J. Emery, Nature **393**, 550 (1998).
- [32] S. Bravyi, B. M. Terhal, and B. Leemhuis, New J. Phys. **12**, 083039 (2010).
- [33] S. Vijay, T. H. Hsieh, and L. Fu, Phys. Rev. X **5**, 041038 (2015).
- [34] I. Affleck, A. Rahmani, and D. Pikulin, Phys. Rev. B **96**, 125121 (2017).
- [35] C. Li and M. Franz, Phys. Rev. B **98**, 115123 (2018).
- [36] Y. Kamiya, A. Furusaki, J. C. Y. Teo, and G.-W. Chern, Phys. Rev. B **98**, 161409 (2018).
- [37] K. Wamer and I. Affleck, Phys. Rev. B **98**, 245120 (2018).
- [38] A. Rahmani, D. Pikulin, and I. Affleck, Phys. Rev. B **99**, 085110 (2019).
- [39] A. Rahmani and M. Franz, Rep. Prog. Phys. **82**, 084501 (2019).
- [40] C. Li, E. Lantagne-Hurtubise, and M. Franz, Phys. Rev. B **100**, 195146 (2019).
- [41] T. Tummuru, A. Nocera, and I. Affleck, Phys. Rev. B **103**, 115128 (2021).
- [42] M. Kamfor, S. Dusuel, J. Vidal, and K. P. Schmidt, J. Stat. Mech.: Theory Exp. **2010**, P08010 (2010).
- [43] E. Quinn, S. Bhattacharjee, and R. Moessner, Phys. Rev. B **91**, 134419 (2015).
- [44] F. Mirmojarabian, M. Kargarian, and A. Langari, Phys. Rev. B **101**, 115116 (2020).
- [45] M. G. Yamada, npj Quantum Mater. **5**, 82 (2020).
- [46] T. Fukui, Y. Hatsugai, and H. Suzuki, J. Phys. Soc. Jpn. **74**, 1674 (2005).
- [47] See Supplemental Material at [URL will be inserted by publisher] for more details.
- [48] S. Pujari, F. Alet, and K. Damle, Phys. Rev. B **91**, 104411 (2015).
- [49] D. Takikawa and S. Fujimoto, Phys. Rev. B **99**, 224409 (2019).
- [50] D. Takikawa and S. Fujimoto, Phys. Rev. B **102**, 174414 (2020).
- [51] D. Takikawa, M. G. Yamada, and S. Fujimoto, (2021), arXiv:2104.11115 [cond-mat.str-el].
- [52] M. G. Yamada and S. Fujimoto, Phys. Rev. Lett. **127**, 047201 (2021).

Supplemental Material for “Quantum liquid crystals in the finite-field KT model for α -RuCl₃”

Masahiko G. Yamada^{1,*} and Satoshi Fujimoto^{1,2}

¹*Department of Materials Engineering Science, Osaka University, Toyonaka 560-8531, Japan*

²*Center for Quantum Information and Quantum Biology, Osaka University, Toyonaka 560-8531, Japan*

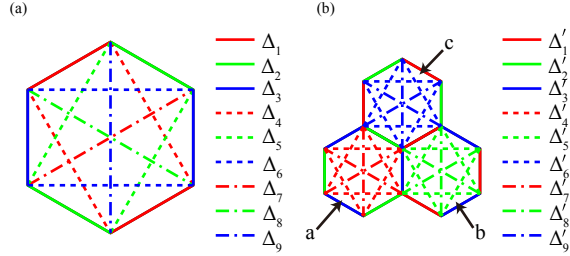


FIG. S1. Definition of order parameters. (a) Order parameters Δ_α for the nematic case. (b) Order parameters Δ'_α for the Kekulé case. Hexagons are labeled *abc* as indicated by arrows.

MEAN-FIELD APPROXIMATION

We here explain the mean-field approximation used in the main text for the effective models. It is important to note that the nematic phase and the Kekulé phase cannot be treated by the same mean-field theory. Thus, we employed two mean-field approximations, each of which is for each bond-ordering pattern. The discussions follow Refs. [1, 2]

The mean-field approximation is done about order parameters Δ_α (and Δ'_α for the Kekulé case) with $\alpha = 1, \dots, 9$ and we assume $\Delta_\alpha = i\langle c_i c_j \rangle$ to be independent of a bond *ij*, where a bond *ij* is defined as shown in Fig. S1 for each Δ_α (and Δ'_α). Correspondingly, we can define τ_α (and τ'_α for the Kekulé case) with $\alpha = 1, \dots, 9$ as a coefficient of the hopping term on the Δ_α bond in the mean-field Hamiltonian. We note that all terms are antisymmetrized in the mean-field Hamiltonian.

Nematic phase

In the nematic case, the mean-field Hamiltonian can be written as

$$H_{\text{MF}} = \sum_{\langle ij \rangle_\alpha} i\tau_\alpha \eta_{ij} c_i c_j, \quad (\text{S1})$$

where $\langle ij \rangle_\alpha$ ($\alpha = 1, \dots, 9$) means that a bond *ij* is connected by the Δ_α -bond, and $\eta_{ij} = \pm 1$ is defined from the antisymmetrization. By diagonalizing this one-body

Hamiltonian, we can obtain a band structure. By filling up the Fermi sea until half filling, we can obtain the mean-field ground state $|\Psi_{\text{MF}}\rangle$ and the mean-field energy $E_{\text{MF}} = \langle \Psi_{\text{MF}} | H_{\text{MF}} | \Psi_{\text{MF}} \rangle$. We note that we need a numerical integration about filled energy bands during the calculation of E_{MF} .

Utilizing the Hellmann-Feynman theorem, we can derive

$$\begin{aligned} \Delta_\alpha &= \frac{1}{N} \frac{\partial E_{\text{MF}}}{\partial \tau_\alpha} \quad (\alpha = 1, 2, 3, 7, 8, 9), \\ \Delta_\alpha &= \frac{1}{2N} \frac{\partial E_{\text{MF}}}{\partial \tau_\alpha} \quad (\alpha = 4, 5, 6). \end{aligned} \quad (\text{S2})$$

Partial derivatives are estimated by numerical differentiation.

The rest is to calculate $E_{\text{tot}} = \langle \Psi_{\text{MF}} | H'_c | \Psi_{\text{MF}} \rangle$. While the free part can directly be written by Δ_α , the interaction energy must be evaluated by Wick's theorem. For example, using an equation like

$$\begin{aligned} i^3 \langle c_1 c_2 c_3 c_4 c_5 c_6 \rangle &= i \langle c_1 c_2 \rangle i \langle c_3 c_4 \rangle i \langle c_5 c_6 \rangle \\ &\quad - i \langle c_1 c_2 \rangle i \langle c_3 c_5 \rangle i \langle c_4 c_6 \rangle \\ &\quad + i \langle c_1 c_2 \rangle i \langle c_3 c_6 \rangle i \langle c_4 c_5 \rangle \\ &\quad - i \langle c_1 c_3 \rangle i \langle c_2 c_4 \rangle i \langle c_5 c_6 \rangle \\ &\quad + i \langle c_1 c_3 \rangle i \langle c_2 c_5 \rangle i \langle c_4 c_6 \rangle \\ &\quad - i \langle c_1 c_3 \rangle i \langle c_2 c_6 \rangle i \langle c_4 c_5 \rangle \\ &\quad + i \langle c_1 c_4 \rangle i \langle c_2 c_3 \rangle i \langle c_5 c_6 \rangle \\ &\quad - i \langle c_1 c_4 \rangle i \langle c_2 c_5 \rangle i \langle c_3 c_6 \rangle \\ &\quad + i \langle c_1 c_4 \rangle i \langle c_2 c_6 \rangle i \langle c_3 c_5 \rangle \\ &\quad - i \langle c_1 c_5 \rangle i \langle c_3 c_4 \rangle i \langle c_2 c_6 \rangle \\ &\quad + i \langle c_1 c_5 \rangle i \langle c_3 c_2 \rangle i \langle c_4 c_6 \rangle \\ &\quad - i \langle c_1 c_5 \rangle i \langle c_3 c_6 \rangle i \langle c_4 c_2 \rangle \\ &\quad + i \langle c_1 c_6 \rangle i \langle c_3 c_4 \rangle i \langle c_2 c_5 \rangle \\ &\quad - i \langle c_1 c_6 \rangle i \langle c_3 c_2 \rangle i \langle c_4 c_5 \rangle \\ &\quad + i \langle c_1 c_6 \rangle i \langle c_3 c_5 \rangle i \langle c_4 c_2 \rangle, \end{aligned} \quad (\text{S3})$$

we can obtain the six-body interaction. Therefore,

$$\begin{aligned}
i^3 \langle c_1 c_2 c_3 c_4 c_5 c_6 \rangle &= -\Delta_1 \Delta_2 \Delta_3 + \Delta_3 \Delta_4 \Delta_5 + \Delta_3^2 \Delta_9 \\
&\quad + \Delta_2 \Delta_4 \Delta_6 + \Delta_4^2 \Delta_7 + \Delta_3 \Delta_4 \Delta_5 \\
&\quad + \Delta_2^2 \Delta_8 - \Delta_7 \Delta_8 \Delta_9 + \Delta_5^2 \Delta_8 \\
&\quad + \Delta_1 \Delta_5 \Delta_6 + \Delta_2 \Delta_4 \Delta_6 + \Delta_6^2 \Delta_9 \\
&\quad + \Delta_1^2 \Delta_7 - \Delta_1 \Delta_2 \Delta_3 + \Delta_1 \Delta_5 \Delta_6 \\
&= -2\Delta_1 \Delta_2 \Delta_3 - \Delta_7 \Delta_8 \Delta_9 \\
&\quad + 2\Delta_3 \Delta_4 \Delta_5 + 2\Delta_2 \Delta_4 \Delta_6 + 2\Delta_1 \Delta_5 \Delta_6 \\
&\quad + (\Delta_1^2 + \Delta_4^2) \Delta_7 + (\Delta_2^2 + \Delta_5^2) \Delta_8 \\
&\quad + (\Delta_3^2 + \Delta_6^2) \Delta_9. \tag{S4}
\end{aligned}$$

A similar reduction is possible for other terms and we can compute E_{tot} . Self-consistent equations can be derived by minimize E_{tot} about τ_α , and by using Eq. (S2). The obtained self-consistent equations are solved iteratively, while each iteration requires diagonalization, numerical integration and numerical differentiation.

Kekulé phase

In the Kekulé case, we consider

$$H'_{\text{MF}} = \sum_{\langle ij \rangle_\alpha} i\tau'_\alpha \eta_{ij} c_i c_j. \tag{S5}$$

In the same way as the nematic case, we can calculate $E'_{\text{MF}} = \langle \Psi'_{\text{MF}} | H'_{\text{MF}} | \Psi'_{\text{MF}} \rangle$.

From the Hellmann-Feynman theorem,

$$\begin{aligned}
\Delta'_\alpha &= \frac{1}{N} \frac{\partial E'_{\text{MF}}}{\partial \tau'_\alpha} \quad (\alpha = 1, 2, 3, 7, 8, 9), \\
\Delta'_\alpha &= \frac{1}{2N} \frac{\partial E'_{\text{MF}}}{\partial \tau'_\alpha} \quad (\alpha = 4, 5, 6). \tag{S6}
\end{aligned}$$

As an illustration, we only compute the six-body term. Differently from the nematic case, the results depend on hexagons. As for the *a*-hexagon defined in Fig. S1(b),

$$\begin{aligned}
i^3 \langle c_1 c_2 c_3 c_4 c_5 c_6 \rangle_a &= -\Delta_3'^3 + \Delta_3' \Delta_4'^2 + \Delta_2' \Delta_3' \Delta_7' \\
&\quad + \Delta_3' \Delta_4'^2 + \Delta_4'^2 \Delta_7' + \Delta_2' \Delta_4'^2 \\
&\quad + \Delta_2' \Delta_3' \Delta_7' - \Delta_7'^3 + \Delta_4'^2 \Delta_7' \\
&\quad + \Delta_3' \Delta_4'^2 + \Delta_2' \Delta_4'^2 + \Delta_4'^2 \Delta_7' \\
&\quad + \Delta_2' \Delta_3' \Delta_7' - \Delta_2'^3 + \Delta_2' \Delta_4'^2 \\
&= -\Delta_2'^3 - \Delta_3'^3 - \Delta_7'^3 \\
&\quad + 3\Delta_4'^2 (\Delta_2' + \Delta_3' + \Delta_7') \\
&\quad + 3\Delta_2' \Delta_3' \Delta_7'. \tag{S7}
\end{aligned}$$

As for the *b*-hexagon,

$$\begin{aligned}
i^3 \langle c_1 c_2 c_3 c_4 c_5 c_6 \rangle_b &= -\Delta_3'^3 - \Delta_1'^3 - \Delta_8'^3 \\
&\quad + 3\Delta_5'^2 (\Delta_3' + \Delta_1' + \Delta_8') \\
&\quad + 3\Delta_3' \Delta_1' \Delta_8', \tag{S8}
\end{aligned}$$

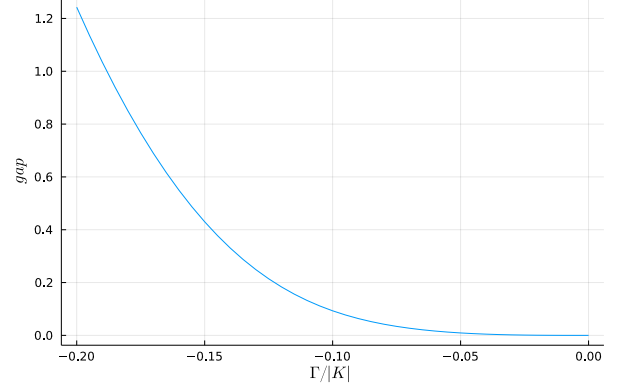


FIG. S2. Gap opening by exact diagonalization.

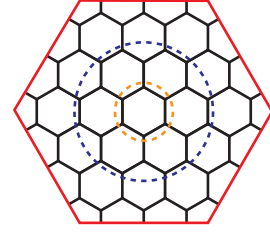


FIG. S3. Entanglement cuts.

Similarly, as for the *c*-hexagon,

$$\begin{aligned}
i^3 \langle c_1 c_2 c_3 c_4 c_5 c_6 \rangle_c &= -\Delta_1'^3 - \Delta_2'^3 - \Delta_9'^3 \\
&\quad + 3\Delta_6'^2 (\Delta_1' + \Delta_2' + \Delta_9') \\
&\quad + 3\Delta_1' \Delta_2' \Delta_9'. \tag{S9}
\end{aligned}$$

By summing up all these terms, we can obtain the expectation value of six-body terms. The derivation and calculation of self-consistent equations are the same as those for the nematic case.

GAP OPENING

As stated in the main text, Kitaev spin liquid may be unstable with respect to a negative Γ perturbatively and it is possible that the Kekulé order opens a gap for Dirac cones. In order to see this we checked the gap opening within the exact diagonalization. On the $h/|K| = 0$ line, the gap opens from $\Gamma/|K| = 0$ to $\Gamma/|K| = -0.2$, as shown in Fig. S2. The original fourfold degeneracy is lifted by an infinitesimal $\Gamma/|K| < 0$.

ENTANGLEMENT ENTROPY

The calculation of entanglement entropy is done by decomposing the Hilbert space as usual. We must be careful

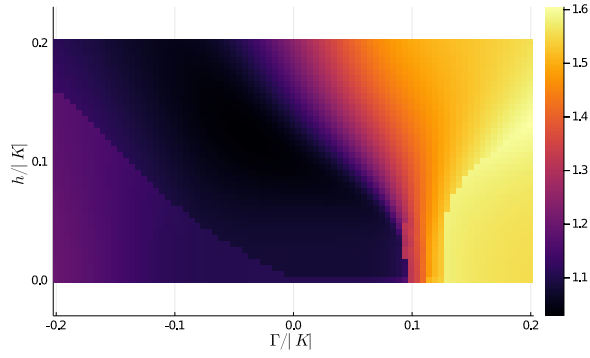


FIG. S4. Entanglement entropy calculated by the 6-site cut for the 54-site system.

about the decomposition because in Majorana systems we cannot cut between a pair of sites, where two Majorana fermions are combined into a complex fermion.

In the 54-site calculation, the entanglement cut is done by 6 sites (orange dashed circle) and 24 sites (blue dashed circle) as shown in Fig. S3. The entanglement entropy calculated by the 24-site cut is shown in Fig. 4 in the main text. The entanglement entropy calculated by the 6-site cut is shown in Fig. S4.

* myamada@mp.es.osaka-u.ac.jp

- [1] C. Li and M. Franz, Phys. Rev. B **98**, 115123 (2018).
- [2] M. O. Takahashi, M. G. Yamada, D. Takikawa, T. Mizushima, and S. Fujimoto, Phys. Rev. Research **3**, 023189 (2021).